



# Oleic and Palmitic Acids with Bioderivatives Essential Oils Synthesized of Spherical Gold Nanoparticles and Its Anti-Human Breast Carcinoma MCF-7 *In Vitro* Examination

Ali Kadhum Bidan<sup>1</sup> · Zainab Shakir Abdullah Al-Ali<sup>1</sup>

Accepted: 31 July 2023 / Published online: 8 August 2023

© The Author(s), under exclusive licence to Springer Science+Business Media, LLC, part of Springer Nature 2023

## Abstract

Gold nanoparticles (AuNPs) have most attention of trend toward treating breast cancer. Especially in overall orientation, essential oils (EOs) considered interested biosource in medicine field and currently in gold nanoparticles synthesizing but EOs concerned to hydrophilic obstacle. Therefore, after creation of AuNPs-based EOs, it converts to hydrophilic for bioapplications rely of spherical, stable, and liked fiber AuNPs surface morphology. EOs-AuNPs observed fight breast cancer MCF-7 cell ability through MTT cytotoxicity assay at half maximal inhibition concentration (IC<sub>50</sub>) at 325 µg/mL. Comet assay in degradation of DNA at 47%, 53% in alkaline, and neutral conditions respectively. Emphasizing rise in apoptosis index was explained in flow cytometry drop populations of treated cells for controlling growth MCF-7 tumor.

**Keywords** Carcinoma MCF-7 · Cytotoxicity · Essential oils · Flow cytometry · Gold nanoparticles

## 1 Introduction

Cancer is more than one disease. It refers to a group of more than 100 distinguish diseases. Although there are many different types of cancer, they all begin when aberrant cells proliferate uncontrollably; cancer is also known as carcinoma [1]. The phrase “breast cancer” refers to all carcinomas of the breast tissue, and it can affect both younger and older females [2]. In a tumor cell’s aberrant metabolism, it has been observed that tumor cells desire a higher glucose metabolism, absorb less oxygen, and produce more lactic acid. As tumor cells deviate their metabolism to anaerobic glycolysis, the morphology of the cells subsequently changes, a phenomenon known as the Warburg effect [3]. Worldwide, breast carcinoma (BC) is the most prevalent. Breast carcinoma (BC) is the most common reason why women die from cancer cause of cancer-related death among females. Internationally, prevalence of BC varies, with some nations having a fivefold higher incidence than others [4]. International Agency for Research on Cancer (IARC) with

its collaborators has evaluated the impact of breast cancer in 2040 and gives a global picture of the disease’s burden in 2020. The authors predict within 2040 pathway incidence of breast carcinoma would result in over three million new cases yearly (40% surge) and over one million fatalities annually (a 50% jump) [5]. BC predicted that up to 40% females with the condition face a recurrence, having greatest probability coming during the first few years following mammary surgery [6]. Hence, tracking cancerous areas with comprehensive therapy is necessary. These comprise chemotherapeutic, hormonal, or immunotherapeutic treatments administered individually or in combination [7]. Regretly, ordinary chemotherapeutic drugs frequently lack target specificity and encourage systemic toxic effects, a wide range of clinical outcomes, and getting rid of quickly dividing cells, including healthy ones resulting in chronic toxicity. This toxicity results in additional side effects including alopecia, thrombocytopenia, and mucositis [8]. In other way, nanotechnology has proved beneficial in the process of identifying, detecting, and eliminating from BC research. Several nanoformulations were produced and researched for eliminating from BC growth, reappearance, or metastases after radiotherapy [9]. Metal nanoparticles (MNPs) are typically consisting primarily of elements or once its oxides core surrounding by an organic or inorganic material or metal oxide shell [10]. Different sized gold nanoparticles are suitable for

✉ Ali Kadhum Bidan  
ali.bidan.sci@uobasrah.edu.iq

<sup>1</sup> Department of Chemistry, College of Science, University of Basrah, Basrah 61004, Iraq

selectively destroying breast cancer cells [11]. Using 14-nm AuNPs as specific looking for drugs to kill mammary cancer cells found a complementary photo-conversion and cellular damage response via doxorubicin. administration [12]. The development of effective techniques significantly steps in the production of AuNPs research priority. The generation of nano gold via biological pattern instance bacteria, fungus, or plantly sources is one of the techniques [13]. Due to its ease of use, quick rate of synthesis, environmental friendliness, and potential to increase biocompatibility with biomolecules, plant-mediated synthesis of Au NPs is notable [14, 15]. The primary benefit of employing extracts is that they are gentle, renewable, and non-toxic reducing and stabilizing agents, which eliminate the requirement for chemical reducing agents [16]. Once biosource of biological technique with continuing interest in nanoparticles creation being essential oils (EOs) is a significant source of bioactive substances. Hence, they are suitable for the synthesis of metallic nanoparticles [17]. The creation of Au NPs has also been achieved with the use of essential oils from other plants. For example, monodispersed hexagonal AuNPs were prepared at room temperature in found essential oils derived from *A. occidentale* leaves [18]. Essential oils defined as conglomeration of dozens of different chemical components, defined principally their volatility, fragrance, low molar mass, and quantity less than one [19]. As a result, it has also been observed that the essential oils extracted from various plant leaves can be particularly effective agents for producing Au at the nanoscale [20]. EOs trigger cancerous cells undergo planned suicide thanks to apoptosis, tissue necrosis, cell cycle termination, and the breakdown of significant membrane compartments. The affected cell's membrane becomes more pliable, coordinating this response, a decrease in energy production, and change of hydrogen exponent; also, destruction of cytochrome capacity is one of the most important precursors to cellular demise [21]. In regarding research, Iraqi *Jasminum sambac* (L.) Aiton leaves were utilized to extract essential oils, with roughly 91% especially oleic acid with palmitic acid and other derivatives of the extracted leaves serving in the preparation of gold in nanoscale, as reducing and capping representatives. Should be emphasized that harvest period, regional origin, hereditary diversity, abiotic (climate, weather, soil), as well as biotic (herbivores, parasites) restrictions can all cause alterations in the composite structure of phytochemicals of *Jasminum sambac* leaves [22]. In spite of essential oils considered to have good medicinal activity, however, their obstacle was concerning as insolubility essential oils in water; therefore, difficulty targeting in vitro mammary cancerous MCF-7 sort. So at this research aimed to overcome solubility, essential oils in water via preparing AuNPs by (EOs) as good solubility in water and strong agent to inhibition MCF-7 cells have grown up. Additionally, *Jasminum*

*sambac* was studied as a promising reducer and capper by using a variant polarity solvent (distilled water) to extract different biomolecules responsible for silver nanoparticle synthesis [23].

## 2 Experimental

### 2.1 Plant Classification

The newly cut of *Jasminum sambac* (L.) Aiton leaves were collected in blossoming farm stretched closing Tigris River in Iraq/Baghdad; it distinguished inside Biology Department, Collage of Science, Basrah University, Basrah, Iraq. *Jasminum* identified as Oleaceae family, the genus *Jasminum*; finally, sort *Jasminum sambac* [24] leaf was trimmed away stem, double rinsed in H<sub>2</sub>O to eliminate pollutants before being washed twice more with deionized water to guarantee no contaminants were present. It is then left to dry for 10 days in the shade (away from light) at 25 °C. The dehydrated samples forwarding to cut into fine smoothed powders using bender. The substance was kept in tight canister under 10 °C for further utilization.

### 2.2 Essential Oils Preparation

*Jasminum sambac* leaf powder was combined with absolute ethanol (EtOH) at a 1:10 ratio and stirred for 2 h at 50 °C before performing double filtration through Whatman filter paper No. 1 under vacuum. When undissolved species were removed, the solution was concentrated using a rotating evaporator at 60 °C. Next, an undergone sample was dried in oven at 60 °C and kept at room temperature for gold nanoparticles preparation.

### 2.3 Preparation and Characterization of H<sub>2</sub>AuCl<sub>4</sub>·3H<sub>2</sub>O

Done preparing H<sub>2</sub>AuCl<sub>4</sub>·3H<sub>2</sub>O in lab from gold 24 karat alloy as source of gold metal considering procedure was described in [25] with shortly modification. H<sub>2</sub>AuCl<sub>4</sub>·3H<sub>2</sub>O characterized by thermogravimetric analysis (TGA) in the Department of Chemistry Education College/University of Basrah, in order to identify molecular formula and purity features.

### 2.4 Physiochemical Instruments

Gold nanoparticles (AuNPs) were characterized by employing spectroscopic instruments, by ultraviolet-visible (UV-VIS) spectroscopy (Shimadzu UV-1800), Fourier transform infrared spectroscopy FTIR (4000–400 cm<sup>-1</sup>) (IRAffinity-1 Shimadzu), X-ray diffraction at an operating voltage of 40

kV, and a current of 30 mA with Cu K radiation ( $\lambda = 0.15406$  nm) (Panalytical X'Pert Pro), to characterize nanomaterials based on nanoscale measurements in addition to other instrumental analysis by gas chromatography/mass spectroscopy GC/MS (Varian/Saturn 2200/USA). An electronic microscope consists of transmission electron microscopy (TEM) and a field emission scanning electronic microscope touched energy dispersive (FESEM-EDX) utilizing device Zeiss. Moreover, AuNPs were evaluated by dynamic light scattering (DLS) and Z-potential with (Malvern) instruments in PH level at 6.5.

## 2.5 Essential Oils Synthesizing Gold Nanoparticles (AuNPs)

Protocol of synthesis of gold nanoparticles (AuNPs)-based essential oils solution was added to  $\text{HAuCl}_4 \cdot 3\text{H}_2\text{O}$  (0.5 mM) according to volume ratio as 1:9 mixed at 25 °C within 120 min away from light, observed changing from ordinary green to raspberry red hue. AuNPs were subjected to a color shift process in a sonicator for a duration of 1 h at a power output of 120 W, resulting in the production of finely distributed particles; to pursue that appoint, it was centrifuged for 50 min at 3500 rpm until separation, then twice washed in distilled water (DW), then repeat centrifugation (for purification) for 30 min. Finally, place it in a vacuum to achieve useful dried AuNPs yields of AuNPs.

## 2.6 Cytotoxicity EOs-AuNPs

MTT is a frequently employed experiment that concentrates on the reduction of 3-(4, 5-dimethylthiazol-2-yl)-2, 5-diphenyltetrazolium bromide (MTT) (yellow tetrazolium dye) to a purple-colored water-insoluble formazan in the mitochondria of living cells. MCF-7 cells have been grown in RPMI-1640 supplemented with 10% fetal bovine serum (FBS), 100 unit/mL penicillin, and 100 g per mL streptomycin. With Trypsin-EDTA, cells were passed, reseeded at 80% confluence twice per week, and incubated at 37 °C. EOs-AuNPs were assessed utilizing MTT colorimetric test [26] finished with several modifications. MCF-7 was grown in 96 vial dish at 4000 cells per vial for 1 day in ideal circumstances (37 °C, 5%  $\text{CO}_2$  within wet container). After removing (10% FBS) medium, these cells had been washed with phosphate-buffered saline twice (PBS). Cells were cultured for 24 h with fresh preservation RPMI media (10% FBS) including (0.05, 0.5, 5, 50, and 500  $\mu\text{g}/\text{mL}$ ) of EOs-AuNPs. At each concentration, triple wells were tested, as well as cylinder elution buffer was used as the reference standard. Each well that received 10  $\mu\text{L}$  of a newly produced solution of 0.5 mg/mL MTT in PBS was stored in 4 h. The medium was withdrawn, and 100  $\mu\text{L}/\text{well}$  of dimethyl sulfoxide was added. To aid in dissolving the formazan crystals, the plates were

softly shaking, using a microplate reader to determine the absorbance value at 545 nm. The mean optical absorbance of the control group as 100%, else categories were determined as a percentage of this value. The ratios of damage to cells as well as the half-maximal inhibitory concentration ( $\text{IC}_{50}$ ) were determined.

## 2.7 DNA Fragmentation of MCF-7

The single-cell gel electrophoresis (SCGE), as described in [27], involved some modifications, which detect DNA strand fractures in eukaryotic cells sequentially. The single-cell gel electrophoresis is a straightforward technique utilized to quantify the occurrence of deoxyribonucleic acid (DNA) segment ruptures in eukaryotic cells. The cells that are enclosed in agarose on a microscope slide undergo lysis through the use of detergent and high salt, resulting in the formation of nucleoids that contain supercoiled loops of DNA that are connected to the nuclear matrix. The application of electrophoresis under high pH conditions leads to the formation of structures that bear resemblance to comets, which can be visualized through fluorescence microscopy. The magnitude of the tail of the comet in relation to its head is indicative of the quantity of DNA breaks. It is likely that loops containing a break undergo a reduction in supercoiling, thus allowing them to elongate unrestrictedly toward the anode. The assay demonstrates a broad spectrum of possible uses, such as assessing the genotoxicity of recently synthesized chemicals, monitoring genotoxic environmental pollution, tracking human biomarkers, and conducting fundamental research in the area of DNA damage and repair. This technique is a straightforward and delicate approach that is commonly executed in animal cells, either in vitro or ex vivo. Nevertheless, it is also feasible to scrutinize DNA impairment in plant cells. The alkaline comet assay is a highly sensitive technique that is capable of detecting minimal levels of DNA damage. The evaluation of DNA recognition was conducted through the utilization of an alkaline for single-strand breaks (SSB) and double-strand breaks (DSB). The MCF-7 cell line was incubated in 25  $\text{cm}^2$  flasks for a duration of 24 h under controlled conditions of (37 °C and 5%  $\text{CO}_2$ ). Subsequently, the subjects were administered with EOs-AuNPs at concentration equivalent to half the inhibitory concentration ( $\text{IC}_{50}$ ) for a duration of 48 h under controlled conditions of 37 °C and 5%  $\text{CO}_2$ . The cells underwent trypsinization, followed by centrifugation at 1000 rpm for 5 min in a new culture medium. Subsequently, they were washed twice with ice-cold PBS that was devoid of Mg and Ca, and centrifuged again at 1000 rpm for 5 min. Following a 24-h treatment with agents, cells ( $1 \times 10^4$ ) were mixed with low melting point agarose (type VII) and subsequently placed onto a glass slide that had been previously coated with high melting point agarose (type I).

Subsequently, the slides were immersed in a lysis solution containing 2.5 M NaCl, 100 mM EDTA, 10 mM Tris base, 1% Triton X-100, and pH 10 and were kept at a temperature of 4 °C for a duration of 60 min. Subsequently, the slides underwent a 30-min rinse in electrophoresis buffer (TBE) at a temperature of 4 °C. Following cell lysis in agarose, DNA was subjected to alkaline treatment (pH >13) for a duration of 30 min to facilitate unwinding, as part of the alkaline staining process. Subsequently, electrophoresis was conducted under controlled conditions with a voltage of 1.0 V/cm and an intensity of 490 mA for a duration of 20 min at a temperature of 4 °C. The staining procedure was conducted utilizing the EtBr (0.5 µg/mL) technique. The assessment involves utilizing the migration distance of DNA as a metric to quantify the extent for DNA impairment within a specific circumstance. Following electrophoresis, the slides underwent a washing process using 0.4 M Tris-HCl (pH 7.5) and were subsequently fixed for a duration of 10 min in absolute alcohol. A total of 100 nuclei were enumerated on every slide, and the proportion of cells exhibiting DNA damage and those without was determined. The cells were segregated into two distinct classifications in the tally, namely intact DNA and impaired DNA. The DNA damage was captured through photographic means using a fluorescence microscope (BX53 Olympus, Germany).

## 2.8 Cell Cycle Arresting of MCF-7

The MCF-7 cells were cultured in 12-well plates using a conventional growth medium, with a seeding density of ( $1 \times 10^5$ ) cells per well. Subsequently, the cells were permitted to adhere for a duration of 24 h, following which the medium was substituted with an exposure medium for a period of

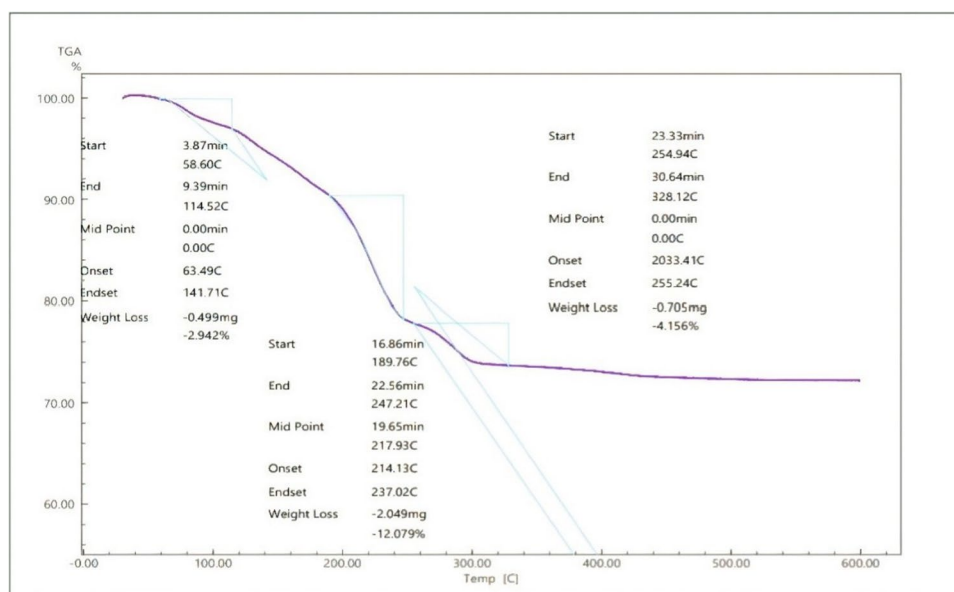
72 h. Subsequently, the exposure medium was replenished at the IC<sub>50</sub> concentration of EOs-AuNPs. Following a 24-h incubation period, cellular specimens were collected and subsequently rinsed with phosphate-buffered saline (PBS). The cell pellets were subjected to staining using a solution of propidium iodide (PI) that was freshly prepared with a volume of 1 ml, consisting of 0.1% Triton X-100, 0.1% sodium citrate, 50g/ml PI, and 10 g/ml of RNase A in PBS. The cells were subjected to storage at a temperature of 4 °C in the absence of light for a duration ranging from 1 h to overnight, prior to their analysis through flow cytometry. The fluorescence spectrophotometer (CyFlow, Partec Co., Germany) was utilized to conduct flow cytometry measurements. Following linear amplification, the collection of PI fluorescence was performed utilizing a band pass filter of 575/25 nm, which corresponds to the orange-red fluorescence (FL2). The capacity of a chemical to induce proliferation, as determined by flow cytometry assay, is reflected by alterations in the proportion of cells in various phases of the cell cycle. The relative proliferative effect percentage (RPE%) was calculated by determining the percentage of cells in the S-phase for EOs-AuNPs in comparison to the negative control.

## 3 Result and Discussion

### 3.1 TGA Interpretation of H<sub>2</sub>AuCl<sub>4</sub>·3H<sub>2</sub>O

Thermogravimetry chart peaks indicated three degradation zones concerned with H<sub>2</sub>AuCl<sub>4</sub>·3H<sub>2</sub>O as shown in (Fig. 1), with values of 2.9% indicating loss of (H<sub>2</sub>O), 12.07% indicating loss of (H<sub>2</sub>O, HCl), and last loss peak of 4.15%

**Fig. 1** Thermogravimetry analysis (TGA) of H<sub>2</sub>AuCl<sub>4</sub>·3H<sub>2</sub>O



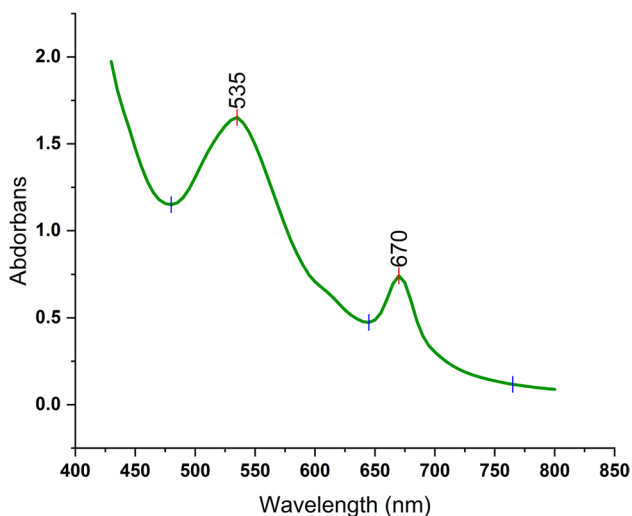


Fig. 2 UV-VIS depicts in determining SPR of EOs-AuNPs

indicating loss of (H<sub>2</sub>O). As AuCl<sub>3</sub> melts at 254.9 °C, the major coordination core is reaming.

### 3.2 UV-VIS Pattern of EOs-AuNPs

Wavelength of gold nanoparticles was evaluated as shown in (Fig. 2) to demonstrate a surface plasmon resonance phenomenon (SPR) maximum absorbance at 535 nm; this evaluation for determining the development of AuNPs, as the maximum absorbance at 535 nm indicated the creation of AuNPs [28]. Phenolic groups in leaves of selected plant which operate as an active principle in reducing and capping gold nanoparticles given SPR spectrum influenced of size and shape AuNPs were created [29]. Appearing small another peak at 670 nm thought due to presenting functional groups with  $\pi$  orbitals; when exposed to ultraviolet-visible radiation, these groups will undergo exciting transitions at the  $\pi$ - $\pi^*$  level in present water as a solvent with remains of polar absolute ethanol mean rising polarity leading to

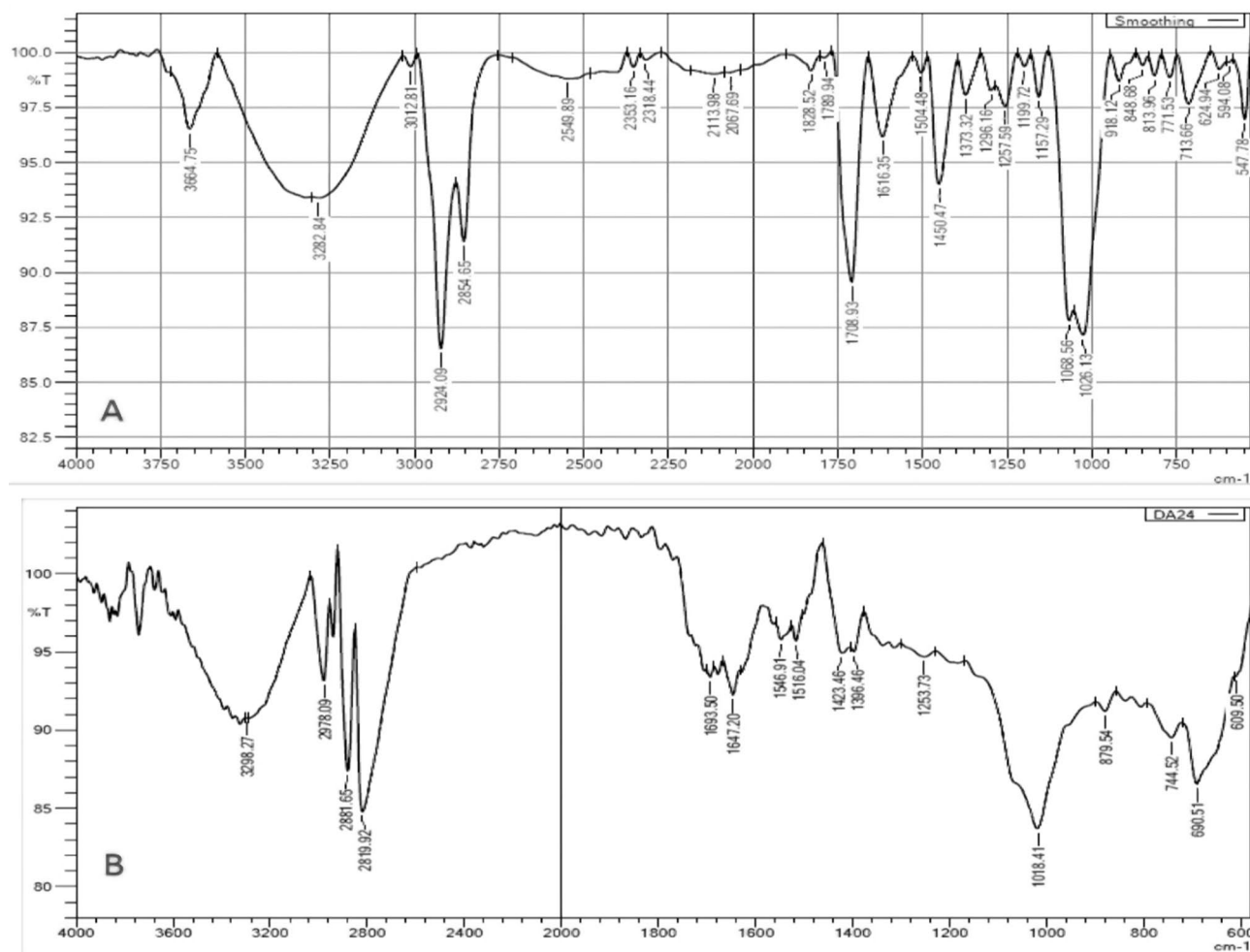


Fig. 3 FTIR charts comparison. A Essential oils soultion. B EOs-AuNPs after bioreduction process

**Table 1** FTIR values data of essential oils in comparison with EOs-AuNPs

Functional groups of essential oils		Functional groups of biosynthesis AuNPs	
Functional group	Frequency $\text{cm}^{-1}$	Functional group	Frequency $\text{cm}^{-1}$
O–H stretching	3282	O–H stretching	3298
O–H bending	1450	O–H bending	1423
C–H stretching	2924	C–H stretching	2819
C=O carboxylic	1708	C=O carboxylic	1647
C–O bending	1068	C=O bending	1081

diminishing energy gap occurring red shift wavelength available between 630 and 670 nm.

### 3.3 FTIR of EOs Solution and EOs-AuNPs

The spectral peaks observed at approximately 3282, 2924, and 1708  $\text{cm}^{-1}$  attributed to the stretching vibration groups of O–H, aliphatic C–H, and C=O, respectively. The peak 1450  $\text{cm}^{-1}$  O–H bending group, while assignment of absorption peaks at 1068  $\text{cm}^{-1}$ , was carried out for C–O group. In opposite side, detected alterations in the nature of biofunctional group of peaks after bioreduction process location was linked to the structure of gold nanoparticle AuNPs, there also a shift in peaks from 1708 to 1693  $\text{cm}^{-1}$  of carbonyl groups and 1450 to 1423  $\text{cm}^{-1}$  of OH groups, as appeared in (Fig. 3), evidence of bioreduction process with creation AuNPs. Their variation shifting in FTIR spectra of the EOs and EOs-AuNPs charts and functional groups were shown in (Table 1) without and with synthesis AuNPs [30]. Hence, modest variations in the transmittance percentage of AuNPs

spectra can be related to the binding of bioactive substances to metal surfaces [31].

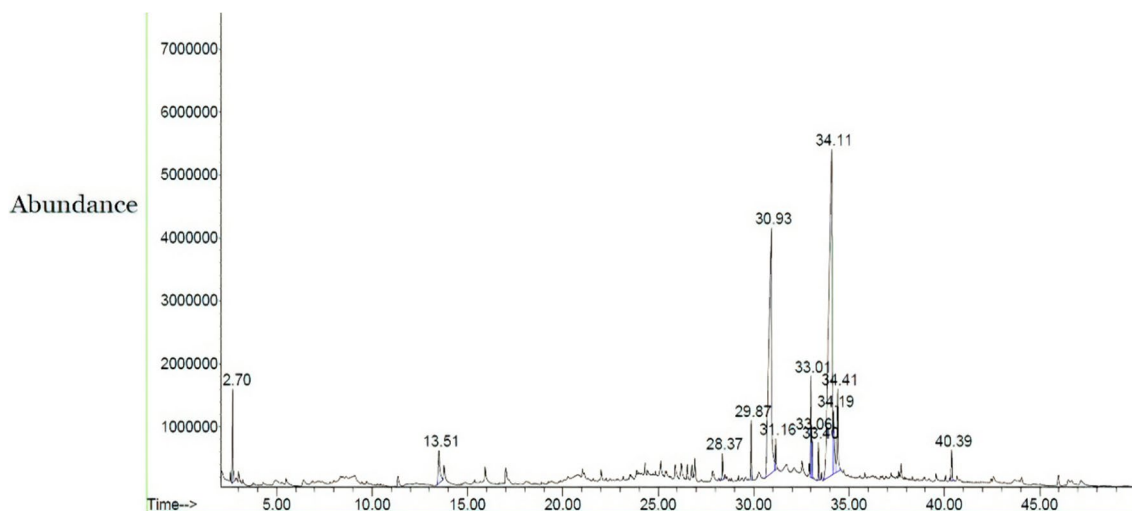
### 3.4 GC-MS Disclosing EOs Structures in Synthesizing AuNPs

Extracted essential oils derived forge about 91% from leaves of selected plant according to GC/MS analysis (Fig. 4) present in majority were oleic and palmitic acids in additionally other essential oils with limited amounts, percents of alcoholic lipids, essential oils act as bioreduction and capping agents which play the majority roles in the bioreduction of  $\text{Au}^{3+}$  ions to  $\text{Au}^0$  nanoparticles. Additional revealed structures were 2.49% of 5-hydroxymethylfurfural participated in capping AuNPs. Another showed structures showed in GC-MS, it cooperates in stabilization-formed AuNPs including propylene glycol, phytol, and elaidolinoleyl alcohol giving totally about 4.84% data of abundance showed in Table 2.

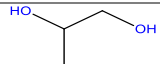
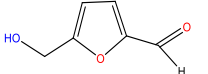
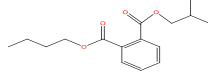
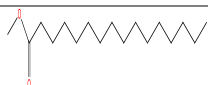


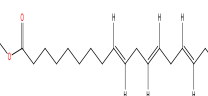

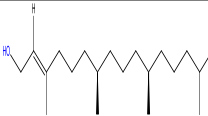
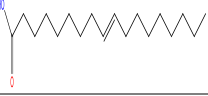
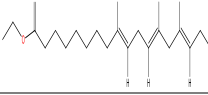

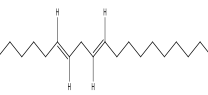
Proposed mechanism to interpretation way of biosynthesis of AuNPs mediated by essential oils illustrated in (Fig. 5).

### 3.5 XRD Diffraction of AuNPs

The crystal structure and phase composition of AuNPs were determined using XRD methods (Fig. 6). The XRD pattern revealed that the essential oils (EOs)-AuNPs were nanocrystalline in nature. Theta locations measured at 38.41°, 44.63°, 64.97°, and 77.98°, which correspond to planes 111, 200, 220, and 311 of reflections of the face-centered cubic (FCC) structure of metallic Au, agree with the literature value (JCPDS card no 00-001-1172) [32]. Background noise was also present, which could be existence of

**Fig. 4** GC-MS analysis biocompounds of essential oils

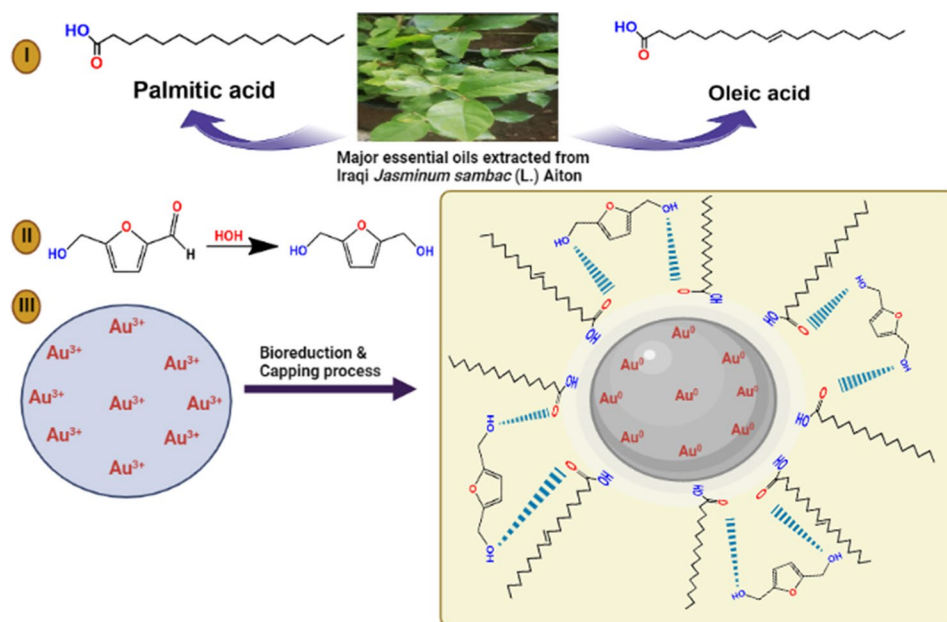
**Table 2** Data values of GC-MS availability of essential oils extracted

No.	Retention time in min	Area of Peak %	Compound identified	Molecular formula	Molecular weight in (g/mol)	Structure
1	2.69	2.51	Propylene glycol	C <sub>3</sub> H <sub>8</sub> O <sub>2</sub>	76.09	
2	13.50	2.49	5-Hydroxymethylfurfural	C <sub>6</sub> H <sub>6</sub> O <sub>3</sub>	126.11	
3	28.37	0.96	1,2-Benzenedicarboxylic acid, butyl 2-methylpropyl ester (Butyl isobutyl phthalate)	C <sub>16</sub> H <sub>22</sub> O <sub>4</sub>	278.34	
4	29.87	1.77	Hexadecanoic acid, methyl ester (Methyl palmitate)	C <sub>17</sub> H <sub>34</sub> O <sub>2</sub>	270	
5	30.93	29.71	Hexadecanoic acid (Palmitic acid)	C <sub>16</sub> H <sub>32</sub> O <sub>2</sub>	256.42	
6	31.16	1.10	Hexadecanoic acid, ethyl ester (Ethyl palmitate)	C <sub>18</sub> H <sub>36</sub> O <sub>2</sub>	284.5	
7	33.01	3.32	9,12,15-Octadecatrienoic acid, methyl ester (α-Methyl linolenate)	C <sub>19</sub> H <sub>32</sub> O <sub>2</sub>	292.5	
8	33.06	1.17	9-Octadecenoic acid, methyl ester (Oleic acid methyl ester)	C <sub>19</sub> H <sub>36</sub> O <sub>2</sub>	296.5	
9	33.40	1.15	Phytol	C <sub>20</sub> H <sub>40</sub> O	296.5	
10	34.11	46.95	9-Octadecenoic acid (Oleic acid)	C <sub>18</sub> H <sub>34</sub> O <sub>2</sub>	282.5	
11	34.19	3.68	9,12,15-Octadecatrienoic acid, ethyl ester (Ethyl linolenate)	C <sub>20</sub> H <sub>34</sub> O <sub>2</sub>	306.5	
12	34.41	4.00	Octadecanoic acid (stearic acid)	C <sub>18</sub> H <sub>36</sub> O <sub>2</sub>	284.5	
13	40.39	1.18	9,12-Octadecadien-1-ol (Elaidolinoleyl alcohol)	C <sub>18</sub> H <sub>34</sub> O	266.5	

related to supplementary bioactive molecules present in the essential oils. As a result, the XRD pattern demonstrates that the AuNPs are crystalline. Employing Scherrer's formula,

the median size of 14 nm computed by the X'Pert High-Score software was applied to determine the diameter of the crystallites.

**Fig. 5** Major biomolecules which are responsible in bioreduction of AuNPs via EOs



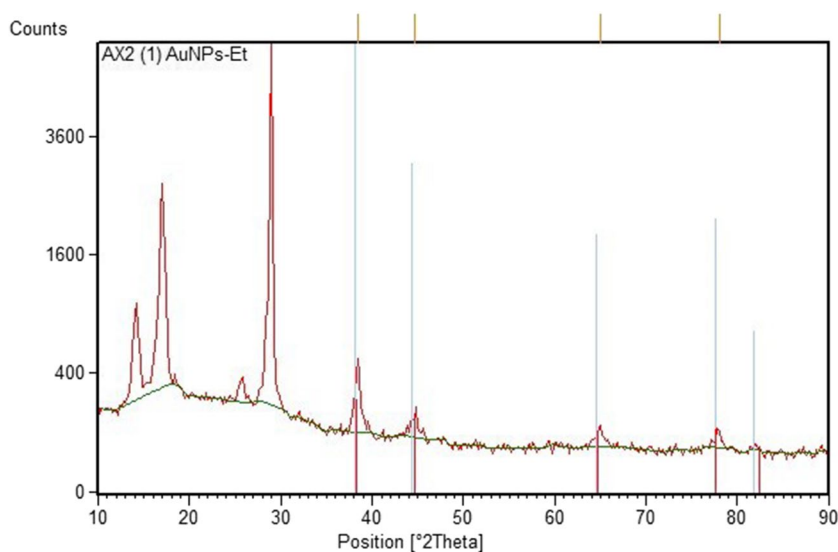
### 3.6 Transmission Electron Microscopy (TEM) Examination of AuNPs

Images of nanomaterials are created by electron beam. This method is used to determine the size and appearance of nano composition. The technique is additionally implemented for the purpose of ascertaining the size spread of nanomaterials [33]. The defined morphology of EOs-AuNPs resembles small spherical particles attached to cloudy regions connected to biomolecules displaying bioreduction, as seen in Fig. 7. The average particle size which was 17.78 nm was examined as the size distribution by Image J software.

### 3.7 FESEM with EDX Explanation of EOs-AuNPs

FESEM is a type of microscope that scans the surfaces of nanomaterials with focused electron beams. This approach provides signals that contain information on the sample's surface topography. It is used for imaging with increased magnification. The plant leaves extract as a reducing and capping agent drastically affected the surface morphology. According to FESEM data, it appeared like fiber geometry of the EOs-AuNPs was used to investigate their surface morphology (Fig. 8). EDX determines the qualitative and quantitative elemental composition of nanomaterials [33].

**Fig. 6** XRD chart diffraction of EOs-AuNPs





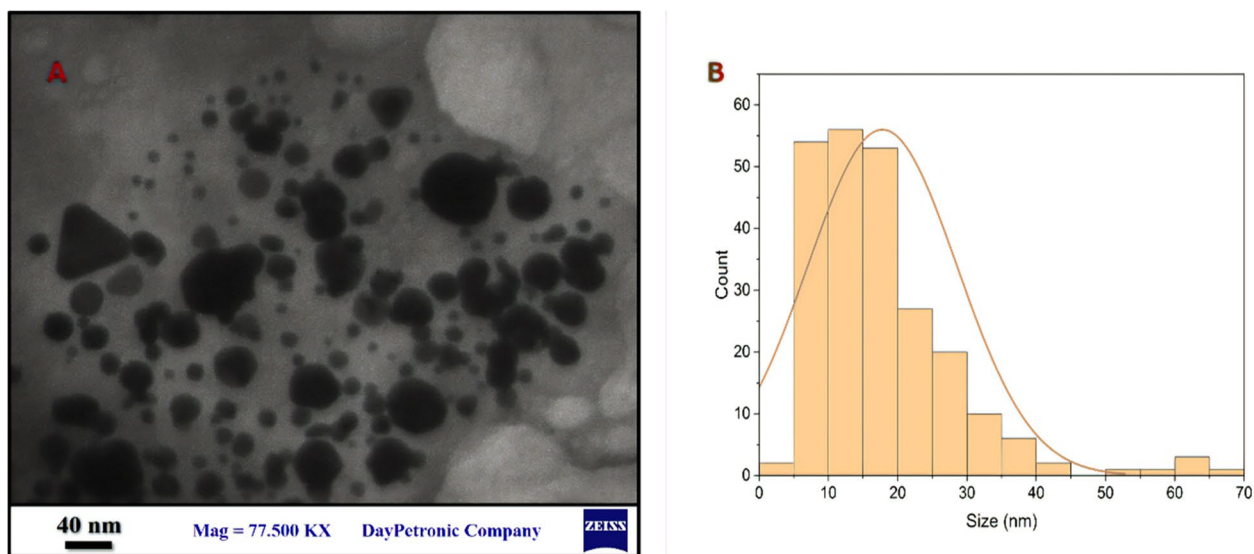


Fig. 7 TEM image depict **A** spherical shape EOs-AuNPs and **B** accounting size distribution of EOs-AuNPs by Imaje J software

As a result, the elemental composition of AuNPs was 94.5 wt.% of Au. The EDX profile revealed an au strong signal for elemental Au at around 2.1 keV. The EDX spectrum also shows tiny peaks for carbon and oxygen with weight percentages of 4.9 and 0.6, respectively. The result of bio-molecules being absorbed by nanoparticle surfaces, resulting in the conversion of Au ions to elemental Au. At the very least, no significant peaks were discovered for synthesized NP. These findings support the spectral evidence for metal ion bio-reduction to metal NPs [34].

### 3.8 DLS and Z-Potential Examination of EOs-AuNPs

DLS is a typical technique for determining particle size distribution. DLS has been demonstrated to be an efficient method for determining the sizes of Brownian nanoparticles in colloidal solutions [35]. DLS uses diffusion coefficients to compute size distribution and nanoparticle mobility [36]. As illustrated in (Fig. 9), the polydispersity index was 0.545, and the hydrodynamic size was estimated to be 498.8 nm. The polydispersity index of the nanoparticles is

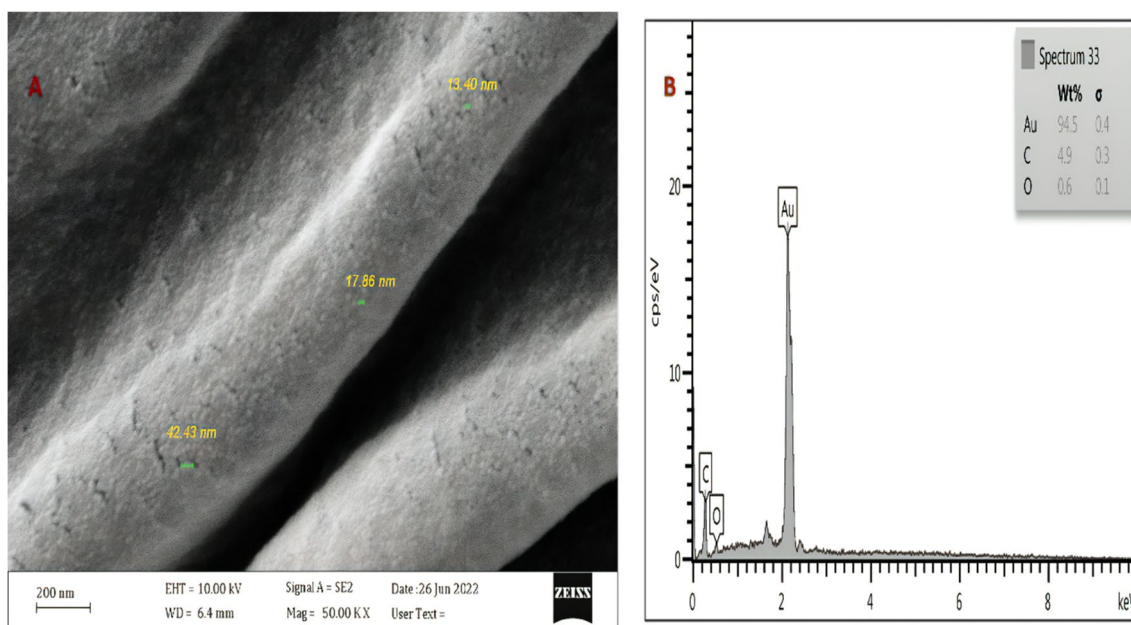
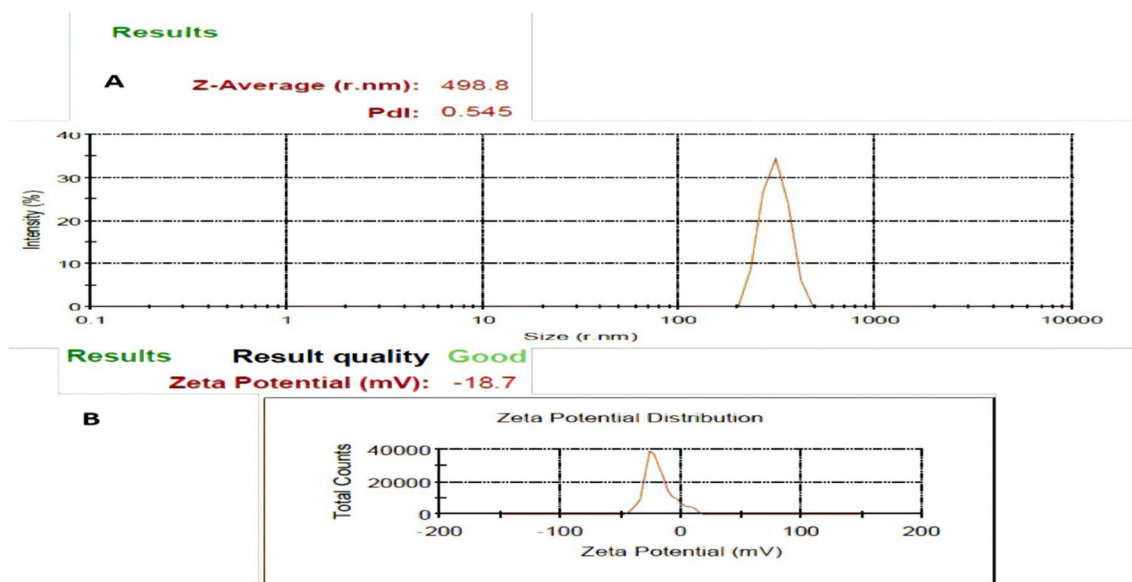


Fig. 8 FESEM showed **A** EOs-AuNPs-like fiber morphology and **B** elemental composition of EOs-AuNPs



**Fig. 9** **A** Dynamic light scattering appears size distribution of EOs-AuNPs. **B** Z-potential examination stability of EOs-AuNPs

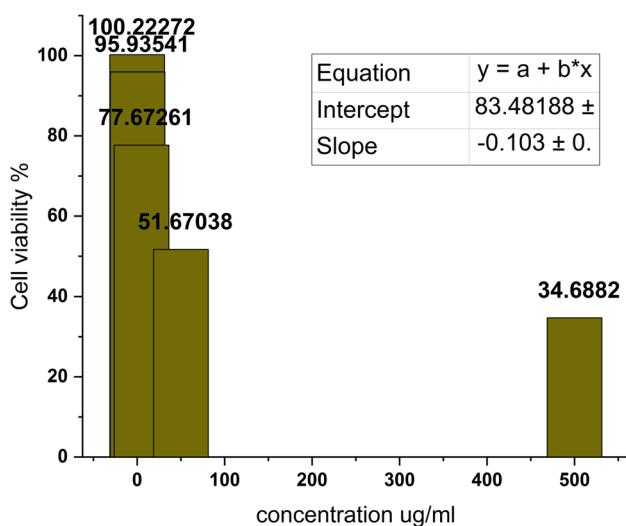
below 0.7, suggesting that they possess superior quality. The determination of the hydrodynamic dimensions and zeta potential of nanoparticles is of paramount importance for prospective research endeavors involving nanoparticles [37]. Upon analyzing the Z-potentials, it can be observed that a significant absolute zeta potential value indicates the presence of electrical charge on the surface of the nanoparticles. The strong repulsive forces exhibited by particles are responsible for preventing their aggregation and thereby ensuring the stability of nanoparticles in the buffer solution [38]. Z-potential had determined at  $-18.7$  mv.

It was determined that gold nanoparticles were relatively stable due to electrostatic repulsion [39].

### 3.9 Cytotoxicity of EOs-AuNPs Against MCF-7 Breast Cancer

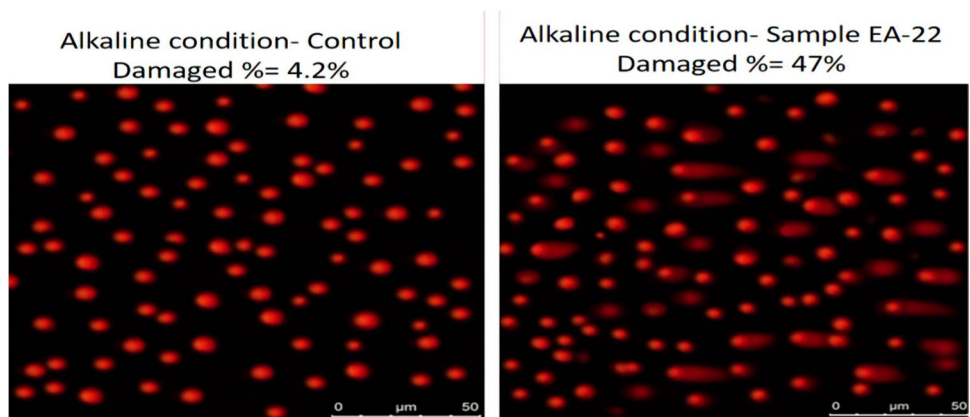
The effect observed which relies on the dosage administered of EOs-AuNPs-produced nanoconjugates on MCF-7 cells was a decline in cell survival and rise in inhibition rate. Measuring percentage for cell viability decreased from 95.9 to 34.6% (between 0.05 and 500  $\mu\text{g/mL}$ ), suggesting that AuNPs had a dose-dependent effect. Within the context of this investigation, many different levels of EOs-AuNPs concentrations involved (0.5  $\mu\text{g/mL}$ , 5  $\mu\text{g/mL}$ , and 50  $\mu\text{g/mL}$ ) were utilized, as stated in the (Fig. 10).

The surface-attached cells grew at a rate of 96–100%. Cellular degradation was seen in MCF-7 cells treated with EOs-AuNPs. The half maximal inhibitory concentration ( $\text{IC}_{50}$ ) of EOs-AuNPs was 325  $\mu\text{g/ml}$ . Cytotoxicity is influenced by numerous variables, incorporating information regarding the specific cancer cell type and the dimensions of the nanoparticle, shape, and surface chemistry [40]. It is believed that the increased cytotoxicity of AuNPs versus malignant cells has a connection with their increased ability for absorption considered in metabolic dysregulation and accelerated growth quantity [41]. In recent years, numerous studies have been conducted to investigate the potential AuNPs generated from variant bio-sources in enhancing cytotoxicity of AuNPs against MCF-7 breast carcinoma cells. One study was preparing AuNPs using *Flaxseed* extract solution, with 1 mM concentration of  $\text{HAuCl}_4 \cdot 3\text{H}_2\text{O}$  for



**Fig. 10** Cytotoxicity data values of treated MCF-7 breast cancer cells by EOs-AuNPs

**Fig. 11** DNA fragmentation of MCF-7 cells by EOs-AuNPs in alkaline media

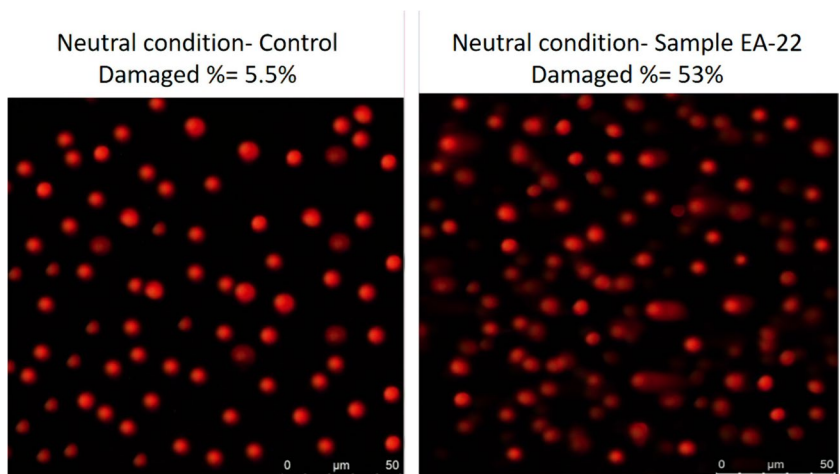


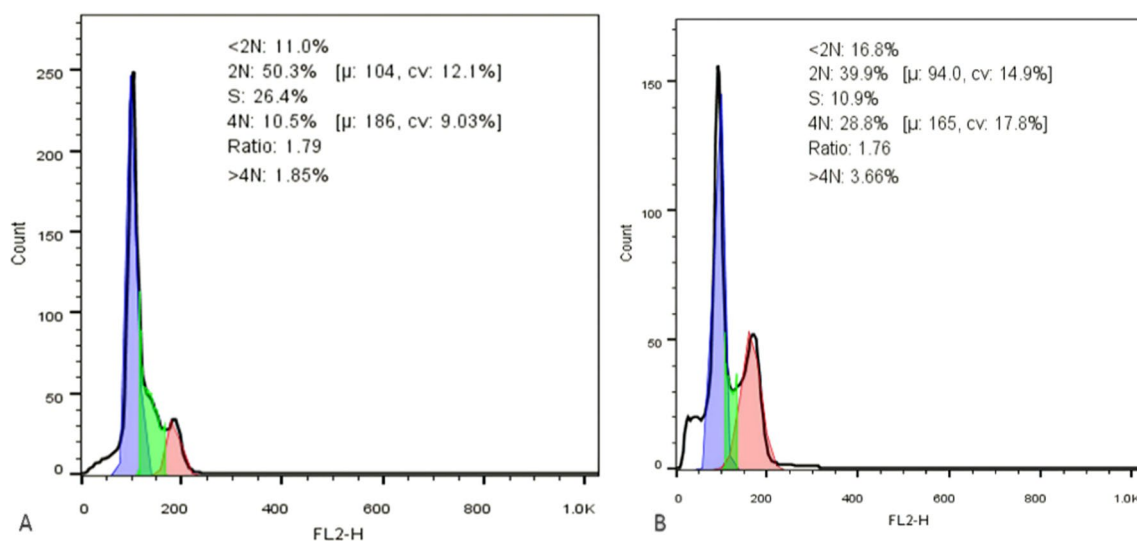
6-h reaction time [42]. Moreover, the study signaled by preparing AuNPs synthesized using the leaf extract of *Enicostema axillare* at a concentration of 1 mM HAuCl<sub>4</sub> for a duration of 24 h. These AuNPs were then evaluated for their potential anticancer properties against breast cancer (MCF-7). The results indicated a reduction in cell viability, suggesting an inhibitory effect on the growth of cancerous cells. These AuNPs have demonstrated promising potential as an anticancer agent against the MCF-7 breast cancer cell line [43]. Else research employed 6-mercaptopurine(6-MP) biomolecule attached to chitosan nanoparticles (CNPs) in present AuNPs (1 mM HAuCl<sub>4</sub> with temperature in boiling level degree) as nano-carrier for creation novel agent fighting MCF-7 cell cancer. The findings indicate that the incorporation of 6-MP into CNPs-AuNPs led to a notable increase in its anti-proliferative effects. This enhancement can be attributed to the improved internalization of 6-MP within cells through the endocytosis mechanism. Consequently, the implementation of interventions has led to a reduction in the adverse effects of 6-MP in the context of cancer therapy [44].

### 3.10 DNA Fragmentation of MCF-7 Cell by EOs-AuNPs

The alkaline comet analysis was conducted to assess capacity for EOs-AuNPs to cause DNA damage in MCF-7 cells. The extent of destruction of DNA which had assessed by measuring the length of the tail was seen in MCF-7 cells exposed to determine IC<sub>50</sub> dose of AuNPs, which were considerable genotoxicity in inhibition of MCF-7 cells by concentration, and was proportionated on rising in DNA fragmentation. Microscope images revealed cells that underwent treatment exhibited tails appearance in comparison to damaged (hidden) head at destroyed percents in alkaline and neutral medias 47% and 53%, respectively, in comparison to control (untreated MCF-7) cells; on the other hand, revealed cell structure decreasing cancer cell population rate reflecting destroyed role of AuNPs as exhibited in (Figs. 11–12). One study has demonstrated that AuNPs can trigger the production of reactive oxygen species (ROS) [45]. A cytotoxicity IC<sub>50</sub> was determined for MCF-7 in order to determine the optimal concentration for the DNA fragmentation assay. This circumstance was also applied to AuNPs mediated by

**Fig. 12** DNA fragmentation of MCF-7 cells by EOs-AuNPs in neutral media





**Fig. 13** **A** Cell cycle arrest of untreated MCF-7 cells. **B** Enhanced apoptosis of treated MCF-7 cells by EOs-AuNPs flow cytometry analysis

*Pterygota alata* (Pa). Thus, Pa–AuNPs suppressed cancer cell proliferation through DNA fragmentation mechanisms that ultimately induced apoptosis [46].

### 3.11 Cell Cycle Arresting Flow Cytometry of EOs-AuNPs

Cell cycle disruption caused by EOs-AuNPs progression in exposing to  $IC_{50}$  concentration of AuNPs was examined after 24 h of treatment. Cell cycle arrest observed drop G1 with S-stage populations, which was associated with an increase in the sub-G1 simultaneously elevated apoptosis index in treated MCF-7 cell by EOs-AuNPs, indicating rapid destruction of, in this investigation, the MCF-7 breast carcinoma cell type (Fig. 13). As a result, cells exposed to AuNPs activated the genotoxicity pathway in measuring to untreated breast cancer cell. This phenomenon associated with the capacity of conjugates to augment the permeation and aggregation of conjugate nanoparticles within MCF-7 type, hence improving the cytotoxicity of the conjugate nanoparticles by decreasing the expression the level of p53 [47]. The extent and nature of cell cycle arrest are contingent upon the composition, dimensions, dispersion, and surface alterations of a cell's components [48]. MCF-7 cells were treated with AuNPs facilitated by *Commiphora wightii*. This treatment has been reported to have the ability to induce apoptosis. The activation of endonucleases and subsequent release of DNA from the cells will increase the number of cells in the sub-G1 phase of the cell cycle technique [49]. Furthermore, El-Deeb and colleagues indicated that the process underlying the anti-cancer properties of the biogenic AuNPs was the ability to induce cell cycle arrest in MCF-7 cells specifically in

the S phase [50]. According to our knowledge, no study or research is concerning combat MCF-7 breast cancer activity relies on AuNPs synthesized by essential oils which were extracted from Iraqi *Jasminum sambac* leaves.

## 4 Conclusion

Essential oils were used to synthesize gold nanoparticles, which are regarded a good source for green synthesis, especially since the bioreduction of AuNPs transformed EOs to hydrophilic state. As a global problem facing humanity, breast cancer necessitated alternative treatment approaches, with AuNPs proving superior to chemotherapy medications. EOs-AuNPs have a spherical form with a size determined by xrd to be 14 nm, TEM to be 17 nm, and DLS to be 498.8 nm. Where, xrd represents the crystalline size of AuNPs, TEM provides the actual size depicted in microscopic image analysis. Variation in size accounting between TEM and DLS is due to the fact that DLS calculates the size of AuNPs with attached biomolecules, which are responsible for the bioreduction process, so the size appears larger in comparison to TEM, which measures the size of AuNPs without additional biomolecules. In the realm of combating breast cancer, AuNPs were found to have a good  $IC_{50}$  cytotoxicity against MCF-7 in vitro cells by destroying the cancer cell's wall. This was developed by conducting a genotoxicity test to demonstrate DNA fragmentation upon reaching the DNA of breast cancer cells. Following that in tracking genotoxicity via cell cycle arrest in observing changeable G0/G1, S-Phase, and G2/M indexes in direction to reduce breast cancer cell divisions for proliferation consequently neutralizes growth of MCF-7 cell directly with growing apoptosis

operation in treated MCF-7 cells. Despite promising pre-clinical outcomes, biosafety and adverse/toxic consequences issues still need to be resolved. Further research must define the immune response to AuNPs formulations and their pharmacokinetic profile.

**Acknowledgements** My sincere appreciation goes to the Chemistry Department of the College of Science at the University of Basrah in Basrah, Iraq. It makes our work more accessible.

**Author Contributions** All authors participated in all manuscript requirements to produce a final version of the manuscript after being read and agreed upon by everyone.

**Funding** Not applicable.

**Data Availability** The data that supports the findings of this study are available within the article.

## Declarations

**Ethical Approval** Not applicable.

**Competing Interests** The authors declare no competing interests.

**Research Involving Humans and Animals Statement** None.

**Informed Consent** None.

## References

- Hanahan, D., & Weinberg, R. A. (2000). *Cell*, 100(2000), 57–70. [https://doi.org/10.1016/S0092-8674\(00\)81683-9](https://doi.org/10.1016/S0092-8674(00)81683-9)
- Russo, J. (2021). *The future of prevention and treatment of breast cancer*. Springer. <https://doi.org/10.1007/978-3-030-72815-1>
- Charnay-Sonnek, F., & Murphy, A. E. (2019). Principle of nursing in oncology: New challenges. *Springer*. <https://doi.org/10.1007/978-3-319-76457-3>
- Alshareeda, A. T., Khatijah, M. N., & Al-Sowayan, B. S. (2022). *Asian Journal Surgery*, 46, 13. <https://doi.org/10.1016/j.asjsur.2022.03.002>
- Arnold, M., Morgan, E., Rumgay, H., Mafra, A., Singh, D., Laversanne, M., Vignat, J., Gralow, J. R., Cardoso, F., & Siesling, S. (2022). *The Breast*, 66, 15–23. <https://doi.org/10.1016/j.breast.2022.08.010>
- Gerber, B., Freund, M., & Reimer, T. (2010). *Deutsches Arzteblatt International*, 107, 85. <https://doi.org/10.3238/arztebl.2010.0085>
- Seidman, A. D., Bordeleau, L., Fehrenbacher, L., Barlow, W. E., Perlmutter, J., Rubinstein, L., Wedam, S. B., Hershman, D. L., Hayes, J. F., & Butler, L. P. (2018). *Journal of Clinical Oncology*, 36, 3259. <https://doi.org/10.1200/JCO.18.00242>
- Razzaghdoust, A., Mofid, B., & Zangeneh, M. (2020). *Journal of Oncology Pharmacy Practice*, 26, 587–594. <https://doi.org/10.1177/1078155219861423>
- Ding, Q., Li, Z., Yang, Y., Guo, G., Luo, F., Chen, Z., Yang, Y., Qian, Z., & Shi, S. (2016). *Drug delivery*, 23, 2677–2685. <https://doi.org/10.3109/10717544.2015.1048490>
- Khan, S. A. (2020). *Metal nanoparticles toxicity: Role of physico-chemical aspects*, in: *Metal nanoparticles for drug delivery and diagnostic applications* (pp. 1–11). Elsevier. <https://doi.org/10.1016/B978-0-12-816960-5.00001-X>
- Ashiq, M. G. B. (2018). *Results in Physics*, 9, 982–986. <https://doi.org/10.1016/j.rinp.2018.03.058>
- Mendes, R., Pedrosa, P., Lima, J. C., Fernandes, A. R., & Baptista, P. V. (2017). *Scientific Reports*, 7, 10872. <https://doi.org/10.1038/s41598-017-11491-8>
- Yazdankhah, M., Veisi, H., & Hemmati, S. (2018). *Journal of the Taiwan Institute of Chemical Engineers*, 91, 38–46. <https://doi.org/10.1016/j.jtice.2018.05.043>
- Varma, R. S. (2014). *Green Chemistry*, 16, 2027–2041. <https://doi.org/10.1039/C3GC42640H>
- Li, S., Al-Misned, F. A., El-Serehy, H. A., & Yang, L. (2021). *Arabian Journal of Chemistry*, 14, 102931. <https://doi.org/10.1016/j.arabjc.2020.102931>
- Sharma, D., Kanchi, S., & Bisetty, K. (2019). *Arabian Journal of Chemistry*, 12, 3576–3600. <https://doi.org/10.1016/j.arabjc.2015.11.002>
- Maciel, M. V. D. O. B., da Rosa Almeida, A., Machado, M. H., Elias, W. C., da Rosa, C. G., Teixeira, G. L., Noronha, C. M., Bertoldi, F. C., Nunes, M. R., & de Armas, R. D. (2020). *Biocatalysis and Agricultural Biotechnology*, 28, 101746. <https://doi.org/10.1016/j.bcab.2020.101746>
- Sheny, D., Mathew, J., & Philip, D. (2012). *Spectrochimica Acta Part A: Molecular and biomolecular spectroscopy*, 97, 306–310. <https://doi.org/10.1016/j.saa.2012.06.009>
- Sharma, M., Grewal, K., Jandrotia, R., Batish, D. R., Singh, H. P., & Kohli, R. K. (2022). *Biomedicine & Pharmacotherapy*, 146, 112514. <https://doi.org/10.1016/j.biopha.2021.112514>
- Ali, S., Iqbal, M., Naseer, A., Yaseen, M., Bibi, I., Nazir, A., Khan, M. I., Tamam, N., Alwadai, N., & Rizwan, M. (2021). *Environmental Nanotechnology. Monitoring & Management*, 16, 100511. <https://doi.org/10.1016/j.enmm.2021.100511>
- Sharifi-Rad, J., Sureda, A., Tenore, G. C., Daglia, M., Sharifi-Rad, M., Valussi, M., Tundis, R., Sharifi-Rad, M., Loizzo, M. R., & Ademiluyi, A. O. (2017). *Molecules*, 22, 70. <https://doi.org/10.3390/molecules22010070>
- Braun, N. A., & Sim, S. (2012). *Natural Product Communications*, 7, 1934578X1200700526. <https://doi.org/10.1177/1934578X1200700526>
- Bidan, A. K., & Al-Ali, Z. S. A. (2022). *International Journal of Nanoscience*, 21, 2250042. <https://doi.org/10.1142/S0219581X22500429>
- Wiersema, J., & Taxonomy, G. (2019). *Checklist Dataset*. <https://doi.org/10.15468/ao14pp>
- Schubert, U., Hüsing, N., & Laine, R. (2008). *Materials syntheses: A practical guide*. Springer Science & Business Media. <https://doi.org/10.1007/978-3-211-75125-1>
- Wang, R., Xing, Z., Wang, M., Gui, Y., & Yang, M. (2020). *Journal of Drug Delivery Science and Technology*, 60, 101975. <https://doi.org/10.1016/j.jddst.2020.101975>
- Singh, N. P., McCoy, M. T., Tice, R. R., & Schneider, E. L. (1988). *Experimental Cell Research*, 175, 184–191. [https://doi.org/10.1016/0014-4827\(88\)90265-0](https://doi.org/10.1016/0014-4827(88)90265-0)
- Yu, J., Xu, D., Guan, H. N., Wang, C., & Huang, L. K. (2016). *Materials Letters*, 166, 110–112. <https://doi.org/10.1016/j.matlet.2015.12.031>
- Alegria, E. C., Ribeiro, A. P., Mendes, M., Ferraria, A. M., Rego, A. M. B. D., & Pombeiro, A. J. (2018). *Nanomaterials*, 8, 320. <https://doi.org/10.3390/nano8050320>
- Morales-Lozoya, V., Espinoza-Gómez, H., Flores-López, L. Z., Sotelo-Barrera, E. L., Núñez-Rivera, A., Cadena-Nava, R. D., Alonso-Núñez, G., & Rivero, I. A. (2021). *Applied Surface Science*, 537, 147855. <https://doi.org/10.1016/j.apsusc.2020.147855>
- Nguyen, T., Huynh, T., Dang, C.-H., Mai, D.-T., Nguyen, T., Nguyen, D.-T., Dang, V.-S., Nguyen, T.-D., & Nguyen, T.-D.

- (2020). *Research on Chemical Intermediates*, 46, 1975–1990. <https://doi.org/10.1007/s11164-019-04075-w>
32. Pawar, C., Sharma, A., Prasad, N., Suryawanshi, S., Nazeruddin, G., Shaikh, V., Kulkarni, A., Al-Sehemi, A. G., & Shaikh, Y. (2022). *Current Research in Green and Sustainable Chemistry*, 5, 100311. <https://doi.org/10.1016/j.crgsc.2022.100311>
33. Bhavyasree, P., & Xavier, T. (2021). *Chemical Engineering Journal Advances*, 8, 100152. <https://doi.org/10.1016/j.ceja.2021.100152>
34. Valsalam, S., Agastian, P., Esmail, G. A., Ghilan, A.-K. M., Al-Dhabi, N. A., & Arasu, M. V. (2019). *Journal of Photochemistry and Photobiology B: Biology*, 201, 111670. <https://doi.org/10.1016/j.jphotobiol.2019.111670>
35. Rafique, M., Shaikh, A. J., Rasheed, R., Tahir, M. B., Bakhat, H. F., Rafique, M. S., & Rabbani, F. (2017). *Nano*, 12, 1750043. <https://doi.org/10.1142/S1793292017500436>
36. Saxena, A., Tripathi, R., & Singh, R. (2010). *Digest Journal of Nanomaterials and Biostructures*, 5, 427–432.
37. Khandel, P., Shahi, S. K., Soni, D. K., Yadaw, R. K., & Kanwar, L. (2018). *Nano Convergence*, 5, 1–17. <https://doi.org/10.1186/s40580-018-0167-9>
38. Sathiyaraj, S., Suriyakala, G., Gandhi, A. D., Babujanarthanam, R., Almaary, K. S., Chen, T.-W., & Kaviyarasu, K. (2021). *Journal of Infection and Public Health*, 14, 1842–1847. <https://doi.org/10.1016/j.jiph.2021.10.007>
39. Shabestarian, H., Homayouni-Tabrizi, M., Soltani, M., Namvar, F., Azizi, S., Mohamad, R., & Shabestarian, H. (2016). *Materials Research*, 20, 264–270. <https://doi.org/10.1590/1980-5373-MR-2015-0694>
40. Qu, X., Yao, C., Wang, J., Li, Z., & Zhang, Z. (2012). *International Journal of Nanomedicine*, 6095–6103. <https://doi.org/10.2147/IJN.S37212>
41. Al Saqr, A., Khafagy, E.-S., Alalaiwe, A., Aldawsari, M. F., Alshahrani, S. M., Anwer, M. K., Khan, S., Lila, A. S. A., Arab, H. H., & Hegazy, W. A. (2021). *Nanomaterials*, 11, 808. <https://doi.org/10.3390/nano1103080>
42. Al-Radadi, N. S. (2021). *Journal of Saudi Chemical Society*, 25, 101243. <https://doi.org/10.1016/j.jscs.2021.101243>
43. Arvindganth, R., & Kathiravan, G. (2019). *Bionanoscience*, 9, 839–847. <https://doi.org/10.1007/s12668-019-00656-6>
44. Faid, A. H., Shouman, S. A., Badr, Y. A., Sharaky, M., Mostafa, E. M., & Sliem, M. A. (2022). *BMC Chemistry*, 16, 1–14. <https://doi.org/10.1186/s13065-022-00892-0>
45. Ahamed, M., Akhtar, M. J., Khan, M. M., Alhadlaq, H. A., & Alrokayan, S. A. (2016). *Environmental Toxicology*, 31, 1344–1356. <https://doi.org/10.1002/tox.22140>
46. Kowsalya, E., MosaChristas, K., Jaqueline, C. R. I., Balashanmugam, P., & Devasena, T. (2021). *Applied Organometallic Chemistry*, 35, e6071. <https://doi.org/10.1002/aoc.6071>
47. Scotti, C., Sommi, P., Paschetto, M. V., Cappelletti, D., Stivala, S., Mignosi, P., Savio, M., Chiarelli, L. R., Valentini, G., & Bolanos-Garcia, V. M. (2012). *PLoS One*, 7. <https://doi.org/10.1371/annotation/c6c16a43-aadd-4cd3-a916-e935534dab38>
48. Kim, J. A., Åberg, C., Salvati, A., & Dawson, K. A. (2012). *Nature Nanotechnology*, 7, 62–68. <https://doi.org/10.1038/nnano.2011.191>
49. Uzma, M., Sunayana, N., Raghavendra, V. B., Madhu, C. S., Shanmuganathan, R., & Brindhadevi, K. (2020). *Process Biochemistry*, 92, 269–276. <https://doi.org/10.1016/j.procbio.2020.01.019>
50. El-Deeb, N. M., Khattab, S. M., Abu-Youssef, M. A., & Badr, A. M. (2022). *Scientific Reports*, 12, 11518. <https://doi.org/10.1038/s41598-022-15648-y>

**Publisher's Note** Springer Nature remains neutral with regard to jurisdictional claims in published maps and institutional affiliations.

Springer Nature or its licensor (e.g. a society or other partner) holds exclusive rights to this article under a publishing agreement with the author(s) or other rightsholder(s); author self-archiving of the accepted manuscript version of this article is solely governed by the terms of such publishing agreement and applicable law.